JOURNAL OF THERMOPHYSICS AND HEAT TRANSFER
Vol. 20, No. 4, October–December 2006

Heat Dissipation with Pitch-Based Carbon Foams and Phase-Change Materials

Kevin W. Wierschke* and M. E. Franke†
Air Force Institute of Technology, Wright–Patterson Air Force Base, Ohio 45433-7765
and
Roland Watts‡ and Rengasamy Ponnappan§
U.S. Air Force Research Laboratory, Wright–Patterson Air Force Base, Ohio 45433-7251

DOI: 10.2514/1.18463

The transient response of pitch-based carbon foam with an infiltrated phase-change material to a step temperature input is described. Pitch-based carbon foams exhibit high thermal conductivities and porosities up to 90%. This allows the possibility of infiltrating the foam with a relatively large volume of phase-change material. Phase-change thermal energy storage devices offer potential weight savings by allowing thermal control systems to use a smaller heat sink by absorbing the thermal energy quickly and storing it in the phase-change material. The thermal energy can then be released to a heat sink and the process repeated. Tests are conducted on samples of infiltrated foam. The results show the transient temperature response of the foam samples before, during, and after phase change. A theoretical prediction of the transient response is developed and compared with the experimental results.

Nomenclature

A	=	area
c	=	specific heat
E	=	energy
E_{stored}	=	energy stored
$\dot{E}$	=	rate of energy transfer
h_{sf}	=	latent heat of fusion
k	=	thermal conductivity
L	=	length
M	=	mass
q	=	heat transfer rate
R	=	thermal resistance
T	=	temperature
t	=	time
τ	=	time constant

Subscripts

C	=	cold side
f	=	foam
H	=	hot side
i	=	initial
in	=	into the region being considered
loss	=	losses
out	=	out of the region being considered
PCM	=	phase-change material
ss	=	steady state

Presented as Paper 5070 at the 38th AIAA Thermophysics Conference, Toronto, Canada, 6–9 June 2005; received 30 June 2005; revision received 20 December 2005; accepted for publication 22 January 2006.

*Captain USAF, Department of Aeronautics and Astronautics, 2950 Hobson Way. Student Member AIAA.
†Professor, Department of Aeronautics and Astronautics, 2950 Hobson Way. Associate Fellow AIAA.
‡Senior Materials Engineer, Nonmetallic Materials Division, 2941 Hobson Way.
§Senior Mechanical Engineer, Power Division, Propulsion Directorate, 1950 Fifth Street. Associate Fellow AIAA.

I. Introduction

THERMALLY conductive carbon foam is showing great promise as a new material for improving the thermal management systems for space and airborne applications. Its characteristics of high thermal conductivity, low density, and high porosity make it ideal to offer potentially significant weight savings while maintaining good thermal performance. Its high porosity allows for a phase-change material to fill the void spaces and create a thermal energy storage system similar to the system proposed by Klett and Burchell [1]. This type of energy storage system is ideal for short duty cycle, high power applications, or applications with oscillatory heat loading. These applications could be as widely varied as burst lasers, thermal protection for spacecraft reentry, or even power amplifiers used in communications systems.

Carbon foam derived from a blown mesophase pitch precursor can be considered to be an interconnected network of graphitic ligaments [2]. These foams consist of an open cell structure and are created through a process of heating and pressurization cycles [3]. The carbon foam with its small pore size and high thermal conductivity allows the selection of phase-change materials without too much concern for the phase-change material's thermal conductivity, as the carbon foam will distribute the heat within the phase-change material. Therefore, the system should be an excellent thermal energy storage device.

Phase-change materials have been in use for temperature regulation by NASA as far back as the lunar rover [1] because of their ability to absorb thermal energy while maintaining a nearly constant temperature during the phase change, therefore, creating a lower system temperature for a short period of time compared with a system without phase-change materials. The ideal phase-change material should have the following characteristics: high heat of fusion, reversible solid to liquid transition, high thermal conductivity, high specific heat and density, long term reliability during repeated cycling, dependable solidifying behavior, low volume change during phase transition, and low vapor pressure [4].

The primary goals for this study are to investigate the transient thermal characteristics of carbon foam with an infiltrated phase-change material, to obtain the experimental time constant and phase-change duration, and to compare some of the experimental results with an analytical model. Secondary goals include the investigation of methods to bond carbon–carbon plates to the carbon foam and to investigate the infiltration methods of the phase-change material.

To determine the transient system performance, a step temperature input was applied to foam samples, with and without infiltrated

phase-change material. Samples of foam were tested with different pore sizes and densities and with different phase-change materials. The response was expected to appear somewhat as a first-order exponential curve with a temperature plateau during the phase change. This exponential curve can be described by the thermal time constant. These parameters, along with the boundary conditions and the duration of the phase-change plateau provide enough information about the response to approximate the thermal response of the infiltrated foam analytically.

II. Methodology

A. Test Article Construction

Graphitized carbon foams from Poco Graphite, Inc., and from Materials and Electrochemical Research (MER) Corporation were used in the experiments. In the particular samples tested, the MER foam was less dense and had larger pore sizes than the Poco brand foam. The foam was cut to $5.6 \times 3.8 \times 2.5$ cm, with the primary direction of heat transfer in the 2.5 cm dimension. The cutting was performed on a high-speed, water-cooled diamond saw. The samples were washed in distilled water and dried to remove any carbon dust or other residue that might prevent good infiltration or bonding. K-800 UNI carbon–carbon composite plates were cut with the diamond saw to 3.8×5.6 cm for bonding on the top and bottom of the sample.

The bond was created using Aremco graphitic bonding material RM-551 which creates a 75% graphite, 25% phenolic resin bond between the foam and each composite plate. The bond was cured using the recommended curing cycle of 2 h at 27°C, 4 h at 129°C, and 2 h at 260°C. After the bond was completed it was inspected under a microscope for thickness and consistency. The bonds used in the test samples averaged approximately 0.025 cm thick. Thinner bonds were created; however, they failed under a slight loading.

Temperatures in the foam were measured with nine imbedded 40-gauge, Teflon-coated copper-constantan thermocouples located as shown in Fig. 1. The thermocouples were bonded to the foam with the same graphitic bonding material as the carbon–carbon plates, but the cure cycle temperature of the bonding material was limited to 149°C due to temperature limitations of the thermocouple wire.

Two phase-change materials were chosen based mainly on a melting point range of 50–100°C for relevance to modern electronics. One was commercial grade paraffin because of its availability and its melting point of 54°C. Its latent heat of fusion is 146 J/g. The other one was acetamide with a melting point of 81°C and a latent heat of fusion of 241 J/g.

Phase-change material infiltration was performed by placing the foam sample to be infiltrated at the bottom of a pool of liquefied phase-change material in a beaker. The beaker was then placed in a vacuum oven and air was removed from the interior of the oven creating a vacuum inside the oven, removing the air from the pores of the foam. Once all the air was removed from the foam sample, indicated by no further bubbling from the sample, the vacuum was released, allowing the liquefied phase-change material to be forced into the foam sample by atmospheric pressure. The foam sample was then allowed to cool to room temperature and removed from the beaker. Excess phase-change material was removed from the foam external surfaces by carefully scraping with a razor blade.

To determine the quality of the infiltration, samples were photographed by a chromo tomography (CT) scanner. The regular test samples were too large to fit in the scanner; therefore, their infiltration was judged by comparison of the percent by volume infiltration of smaller samples that could fit in the scanner. In Fig. 2 the infiltration can be seen in a CT scan image of a small sample. Dark spots in the center of the foam are voids not filled by the phase-change material. Carbon–carbon plates can be seen as solid lines on the top and bottom of the image.

The hot side of the regular test sample was on the bottom of the schematic sample shown in Fig. 1 and the insulated or cold side was on top. The four open sides of the regular test samples were sealed with 828 epoxy resin. This was done by placing the sample in a mold and covering with the liquid resin. The resin was then cured under vacuum. By curing under vacuum, the air in the foam where phase-change material could not infiltrate was removed, leaving voids in the cured test sample. These voids are a necessary part of the sample as they allow the phase-change material expansion room. The resin was then sanded down to expose the carbon–carbon plates on the top and bottom of the sample for good contact with the hot and cold plates of the experiment.

B. Experimental Apparatus and Procedure

The experimental apparatus, Fig. 3, provided a transient one-dimensional heat flow to or through the experimental sample. The

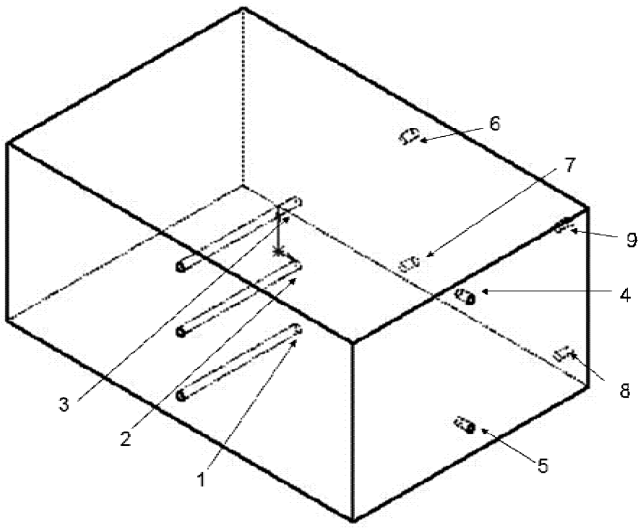

Fig. 1 Thermocouple locations.

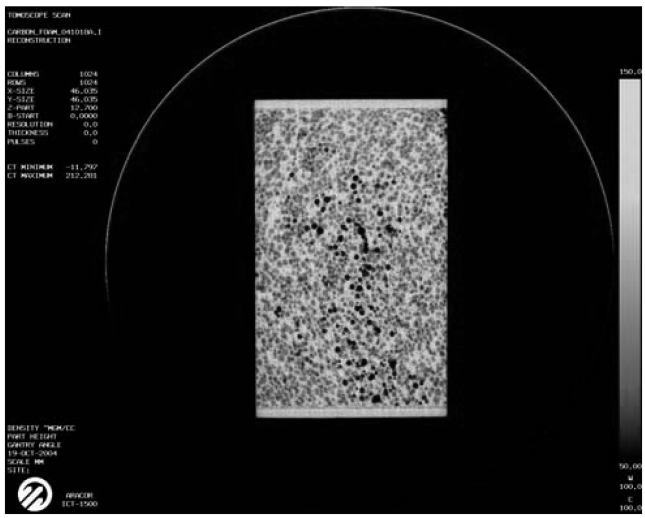

Fig. 2 CT scan of phase-change material infiltration.

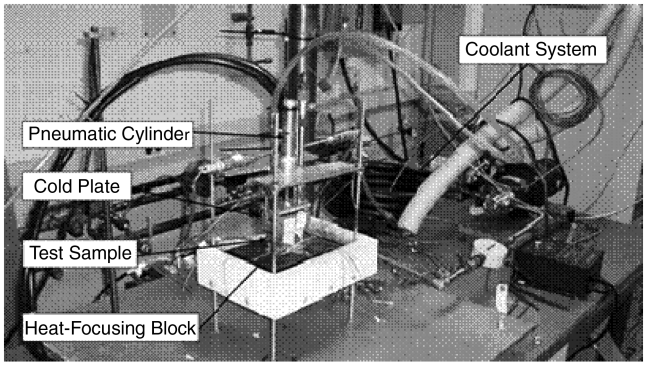

Fig. 3 Photograph of experimental apparatus.

Table 1 Experimental scenarios

Foam type	Boundary conditions	Phase-change material	Boundary temperature T_H, °C
MER	Insulated	Empty	70
MER	Insulated	Empty	95
MER	Insulated	Acetamide	95
MER	Insulated	Paraffin	70
MER	Cooled	Empty	95
MER	Cooled	Empty	135
MER	Cooled	Acetamide	135
MER	Cooled	Paraffin	95
Poco	Insulated	Empty	70
Poco	Insulated	Empty	95
Poco	Insulated	Acetamide	95
Poco	Insulated	Paraffin	70
Poco	Cooled	Empty	95
Poco	Cooled	Empty	135
Poco	Cooled	Acetamide	135
Poco	Cooled	Paraffin	95

heater consisted of an oxygen-free copper heat-focusing block with 11 one-kilowatt heater cartridges inside. This copper block was instrumented with thermocouples to measure the power flowing out of the copper block into the foam test sample.

A nonlinear feedback control system was constructed to maintain the copper block at a constant temperature. This controller has two modes. First, the heat-up mode heated the block to within 5°C of the desired temperature using 500 W of power. Once the copper was within 5°C, the control system shifted modes to the temperature maintenance mode. This mode added a controlled amount of power based on the power going into the foam and the temperature of the copper block. The data acquisition unit limited the performance of this controller as the data acquisition unit only sampled once every 4 s. This performance limitation allowed the copper to drop 2–4°C upon initial application of the foam sample before the controller reacted to raise the temperature back to the desired temperature.

In the second setup the top of the foam sample was attached to a cold plate for heat removal. The temperature of the cold plate was maintained at a constant temperature of 25°C by a flow of poly-alphaolefin (PAO), a coolant used in aircraft. The cold plate and foam sample were attached to a pneumatic cylinder, which placed and removed the foam sample on the heat-focusing plate. The pneumatic cylinder allowed this placement to happen repeatedly. It also held the sample with consistent pressure on the heat-focusing block. A flexible attachment of the pneumatic cylinder automatically adjusted for the sample being slightly out of square, producing a solid, even contact of the foam sample with the heat-focusing block and cold plate.

This entire setup was designed to apply a step temperature input to the foam sample. With a step temperature input, the transient temperature profile was measured and the system's time constant and phase-change duration were calculated. The experiments were performed with two different foams, two different phase-change materials or none, and three different heater temperatures. The boundary conditions were varied depending on the melting point of the phase-change material, but also changed by insulating the sample from the cold plate or bringing it in direct contact with the cold plate as previously described. These combinations created 16 different test conditions, which are listed in Table 1.

C. Test Configuration and Theory

To predict the transient response, an energy balance was considered that depended on two categories of boundary conditions, the insulated and the cooled cases. In the insulated case, the foam test sample with and without phase-change material was insulated on all sides except where it came into contact with the copper heat-focusing block. The cooled scenario consisted of the test sample with the copper heat-focusing block on the bottom, the cold plate on the top, and fiberglass insulation on the other four sides.

For this study T_H was measured just inside the copper heat-focusing block. The temperature of the foam was measured at nine different places in the foam as indicated in Fig. 1. For theoretical predictions the temperature was assumed to be uniform across the foam, and T_C was measured in the PAO coolant.

There are three distinct portions of the temperature curve, which must be solved for separately: first, the initial rise before the sample has reached the phase-change materials' melting point; second, the plateau where the phase-change material melts; and third, the final rise where the phase change has occurred and the sample is increasing in temperature again. These portions were predicted by solving for the time constant of the portion of the curve when the phase-change material is solid and liquid, solving for the duration of the phase change, and finally assembling the three predictions.

To determine the analytic response of the foam, a lumped capacitance method similar to that employed by Incropera and DeWitt [5] was used. The thermal resistance from the boundary conditions to the foam sample was determined by setting up a thermal resistance network and solving for the total resistance. This was done on the hot side and the cold side of the foam sample.

On the hot side the heat must flow through a section of copper, a contact joint with phase-change thermal grease, the carbon–carbon plates, a layer of bonding material, and finally foam with or without phase-change material. In a resistance network the joint resistance looks like that shown in Fig. 4.

The copper resistance, the carbon–carbon plate resistance, the bonding material resistance, and the foam resistance were calculated using Eq. (1).

$$R = \frac{L}{kA} \tag{1}$$

The resistance of the phase-change grease was obtained from the manufacturer's specifications. The total resistance R_H was calculated by summing each individual resistance in series.

On the cold side, the heat must flow through a section of carbon foam, the bonding material, the carbon–carbon plate, the phase-change thermal grease, a copper plate, through an offset fin heat exchanger to the PAO coolant. This is shown in a resistance network schematic in Fig. 5.

Once again the copper, carbon–carbon plate, bonding material, and the foam resistances were calculated. The thermal resistance from the copper plate to the PAO through a copper fin array was obtained from Cao and Ponnappan [6]. The total resistance R_C is the summation of the separate resistances, including the phase-change grease resistance.

These resistance calculations only represent a lower bound estimate for the actual thermal resistance. The actual thermal resistance will include a contact resistance, between the carbon–carbon plate and the copper, most reliably determined experimentally due to the complexity of contact resistance [5]. Estimates for R_H and R_C are required for solving for the time constants. A second approach to determining the resistance was to use experimentally calculated values for R_H and R_C.

To solve for the time constants, first, consider the case where the sample is heated but is insulated from the cold plate. If we assume perfect insulation there is no heat flux out of the sample ($\dot{E}_{\text{out}} = 0$). The energy rate balance ($\dot{E}_{\text{in}} - \dot{E}_{\text{out}} = E_{\text{stored}}$) then becomes

Fig. 4 Thermal resistance network (hot side).

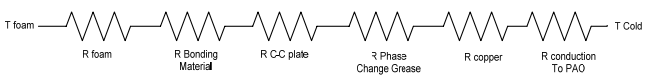

Fig. 5 Thermal resistance network (cold side).

$$q_{\text{in}} = (M_f c_f + M_{\text{PCM}} c_{\text{PCM}}) \frac{\mathrm{d}T}{\mathrm{d}t} \tag{2}$$

where q_{in} is described by

$$q_{\text{in}} = \frac{T_H - T_f}{R_H} \tag{3}$$

By solving Eq. (2) with Eq. (3), an expression for the temperature of the foam as a function of time is given by

$$T_f = T_H - (T_H - T_{fi}) e^{-[t/R_H(M_f c_f + M_{\text{PCM}} c_{\text{PCM}})]} \tag{4}$$

where a time constant can be defined as

$$\tau = R_H (M_f c_f + M_{\text{PCM}} c_{\text{PCM}}) \tag{5}$$

For the second case where the foam block is placed against the cold plate and the heat flux out is no longer zero, the energy rate balance becomes

$$q_{\text{in}} - q_{\text{out}} = (M_f c_f + M_{\text{PCM}} c_{\text{PCM}}) \frac{\mathrm{d}T}{\mathrm{d}t} \tag{6}$$

By substituting Eq. (3) and

$$q_{\text{out}} = \frac{T_f - T_c}{R_c} \tag{7}$$

into Eq. (6), the energy rate equation becomes

$$\frac{R_c T_H + R_H T_c}{R_c R_H} - \frac{R_C + R_H}{R_C R_H} T_f = (M_f c_f + M_{\text{PCM}} c_{\text{PCM}}) \frac{\mathrm{d}T}{\mathrm{d}t} \tag{8}$$

Solving this equation is slightly more complex. It can, however, be solved by the use of integrating factors where the expression for the temperature of the foam becomes

$$T_f = \frac{R_C T_H + R_H T_C}{R_C + R_H} + \left(T_{fi} - \frac{R_C T_H + R_H T_C}{R_C + R_H} \right) \times e^{-[(R_C + R_H)/R_C R_H (M_f c_f + M_{\text{PCM}} c_{\text{PCM}})]t} \tag{9}$$

From this, the time constant for the cooled case can be defined as

$$\tau = \frac{R_c R_H (M_f c_f + M_{\text{PCM}} c_{\text{PCM}})}{R_c + R_H} \tag{10}$$

In either case, this is not the complete solution for the transient response because the phase-change plateau must also be solved.

Once the system reaches the melting point of the material, the system temperature will plateau for a short time while the phase change takes place. This time can be calculated by starting with an energy balance on the foam sample. By drawing a control volume just inside the foam sample, the energy balance equation is

$$E_{\text{in}} - E_{\text{out}} = E_{\text{stored}} \tag{11}$$

Letting $E_{\text{in}} = q_{\text{in}} t$, $E_{\text{out}} = q_{\text{out}} t + q_{\text{loss}} t$, and $E_{\text{stored}} = M_{\text{PCM}} h_{\text{sf}}$, the energy balance becomes

$$q_{\text{in}} t - (q_{\text{out}} t + q_{\text{loss}} t) = M_{\text{PCM}} h_{\text{sf}} \tag{12}$$

The phase-change time from Eq. (12) becomes

$$t_{\text{phase change}} = \frac{M h_{\text{sf}}}{q_{\text{in}} - q_{\text{out}} + q_{\text{loss}}} \tag{13}$$

After solving for the time constant and the duration of the phase change, the predicted transient temperature profile can be assembled for each case. Using this temperature profile as T_f, the power flowing into the foam can be predicted using Eq. (3).

III. Results and Analysis

A. Bonding Results

During bonding the ultimate goal is to reduce the thermal resistance, allowing heat to flow easily. The thermal resistance is calculated by Eq. (1). The bonding material fixes k, and A is fixed by the geometry of the test sample. Therefore, to minimize the thermal resistance of the bond, L must be kept to a minimum. By viewing under a microscope, the bond can be seen and inspected for thickness, voids, and consistency.

In Fig. 6 a bond can be seen between the carbon–carbon plate on the bottom and the carbon foam on the top. Small voids can be seen near the edge of the foam sample. Voids will reduce the area of the bond, and therefore increase the thermal resistance of the bond. The bond is approximately 0.013 cm thick with numerous voids. This attempt at bonding failed and was judged to be too thin.

The second attempt at bonding can be seen in Fig. 7. This bond is thicker and has fewer voids. This bond is approximately 0.025 cm thick and strong enough that the carbon–carbon plates fail before the bond breaks. Without moving to more precise and complex techniques for creating the bond, the 0.025 cm thick bond was accepted to minimize the thermal resistance and still be strong enough to secure the upper and lower plates to the foam.

B. Infiltration Results

Chromo tomography scans were used to judge the infiltration. CT scans allowed the infiltration to be seen without damaging the sample itself. Each image shown in Fig. 8 represents a *slice* at a different depth of the sample. The carbon–carbon plates can be seen on the top

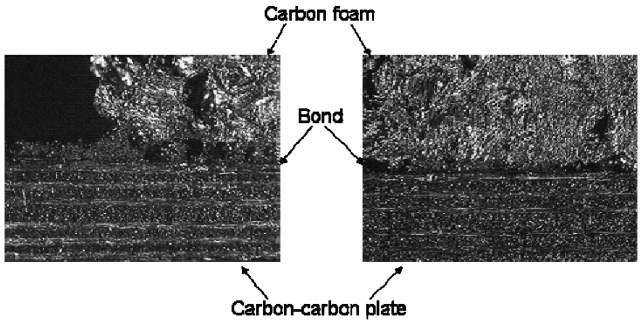

Fig. 6 Images of first bond (sample edge, left; in middle; right).

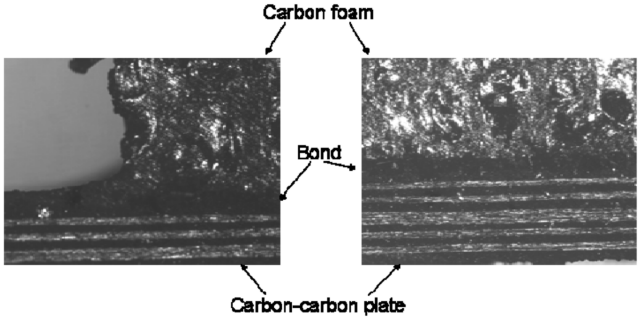

Fig. 7 Images of second bond (sample edge, left; in middle, right).

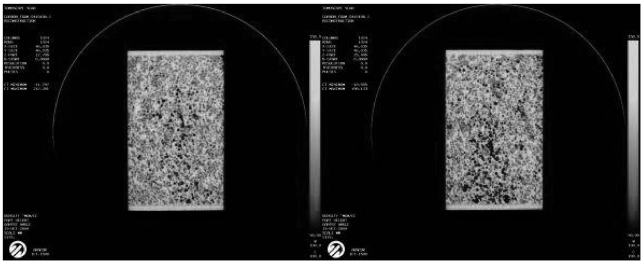

Fig. 8 CT scan of phase-change material infiltration.

and bottom. The black areas are voids in the foam that were not infiltrated with the phase-change material. This sample is 42% by volume phase-change material, a complete enough infiltration to be used for the experimental samples.

The experimental regular samples were infiltrated using the same technique and had similar results based on weight measurements. The infiltration percentages are shown in Table 2. The MER foam was less dense and more easily infiltrated than the Poco foam.

C. Predicted and Experimental Results

The experimental time constants were obtained from the data by performing a curve fit on the center thermocouple data, thermocouple number 2, during the transient portion of the experiment. This transient portion was considered the portion where the temperature of the foam sample was less than 99% of the final temperature in the empty sample scenarios. When the foam sample was infiltrated with phase-change material, the time constant was determined from data less than 10°C below the phase-change temperature. By only using this portion of the curve the curve fit was performed without incorporating the effects of the phase change. The time constant was obtained from

$$T(t) = T_{ss} - (T_{ss} - T_i)e^{-t/\tau} \tag{14}$$

where T_{ss} is the maximum temperature the sample reaches during the test and T_i is the temperature of the foam sample before heat is added. This process was repeated for each experimental scenario. The time constants for the experimental scenarios are given in Table 3.

Predicted time constants were generally smaller than the curve fit time constants. This comparison is shown in Table 3. This difference is expected to come from two sources. First, the resistances predicted were a lower bound estimate only. If these values were increased, the predicted time constant would be larger and the response slower. This hypothesis was tested by calculating a predicted time constant using the method described in the Test Configuration and Theory section, but replacing the resistance calculated using the resistance network with experimentally determined resistances. These experimental resistances were calculated from the experimental data at each point using Eqs. (15) and (16). Table 3 shows that the time constants calculated using the experimentally determined resistances produce a somewhat more accurate solution on average.

$$R_H = \frac{T_{copper} - T_{foam}}{q_{in}} \tag{15}$$

$$R_C = \frac{T_{foam} - T_{PAO}}{q_{out}} \tag{16}$$

Other possible differences between experimental and predicted time constants come from approximations and simplifications made during the theoretical analysis, including values selected for the specific heats of the foam and phase-change material, nonuniform

Table 2 Infiltration results

Sample	Infiltration by volume, %
Poco A: Paraffin	48.99
Poco B: Acetamide	54.27
Poco C: Paraffin	44.44
Poco D: Paraffin	48.26
MER 1: Paraffin	63.70
MER 3: Acetamide	63.77

Table 3 Predicted vs experimental time constants

Foam Type	Boundary conditions	Infiltrated medium	Boundary temperature T_H, °C	Curve fit time constant, min	Predicted time constant theoretical, min	Percent different	Predicted time constant Experimental R, min	Percent different
MER	Insulated	Empty	70	0.36	0.21	41	0.20	45
MER	Insulated	Empty	95	0.40	0.21	47	0.23	41
MER	Insulated	Acetamide	95	0.80	0.64	20	0.55	32
MER	Insulated	Paraffin	70	0.68	0.69	1	0.51	25
MER	Cooled	Empty	95	0.27	0.17	37	0.26	3
MER	Cooled	Empty	135	0.27	0.17	37	0.26	2
MER	Cooled	Acetamide	135	1.07	0.51	52	1.14	7
MER	Cooled	Paraffin	95	0.96	0.55	43	0.81	16
Poco	Insulated	Empty	70	0.47	0.32	31	0.48	3
Poco	Insulated	Empty	95	0.51	0.32	36	0.32	37
Poco	Insulated	Acetamide	95	1.30	0.71	45	0.75	42
Poco	Insulated	Paraffin	70	0.95	0.70	27	0.76	20
Poco	Cooled	Empty	95	0.40	0.26	36	0.31	21
Poco	Cooled	Empty	135	0.42	0.26	39	0.40	5
Poco	Cooled	Acetamide	135	0.56	0.56	1	1.15	106
Poco	Cooled	Paraffin	95	0.64	0.55	14	0.47	27
					Average	32		27

Table 4 Predicted vs actual phase change time

Foam type	Boundary conditions	Infiltrated medium	Boundary temperature T_H, °C	Actual phase change time, min	Predicted phase change time, min	Percent different	Predicted time for phase change Experimental R, min	Percent different
MER	Insulated	Acetamide	95	5.0	4.1	18	3.5	30
MER	Insulated	Paraffin	70	2.0	1.6	20	1.2	42
MER	Cooled	Acetamide	135	5.0	1.4	73	3.1	39
MER	Cooled	Paraffin	95	1.6	0.7	54	1.3	20
Poco	Insulated	Acetamide	95	3.8	3.5	6	3.8	1
Poco	Insulated	Paraffin	70	2.5	1.2	51	1.3	46
Poco	Cooled	Acetamide	135	3.1	1.2	63	2.5	20
Poco	Cooled	Paraffin	95	1.1	0.6	48	0.6	48
					Average	42	Average	27

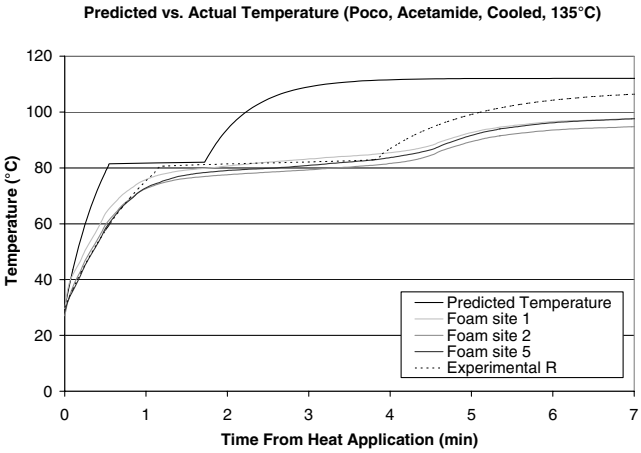

Fig. 9 Predicted vs actual temperature profile.

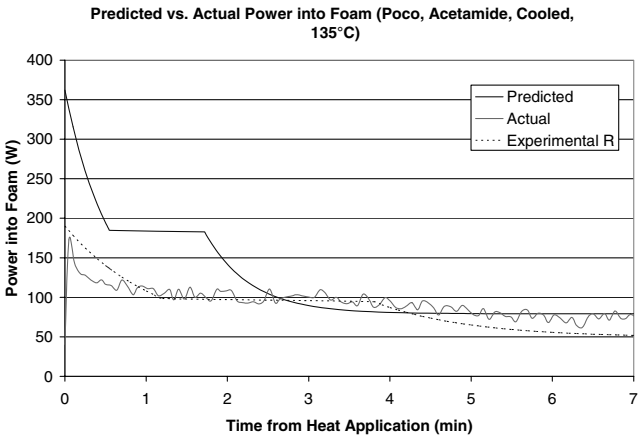

Fig. 10 Predicted vs actual power.

infiltration throughout the foam, and heat losses through the sides of the foam samples.

The predicted and experimentally determined phase-change times are listed in Table 4. The prediction of the phase-change time was consistently shorter than the experimental results as shown in Table 4. Again, the thermal resistances calculated from the predicted individual resistances were the source of some of the error. The phase-change times were recalculated using the experimentally determined resistance to show improved phase-change times with improved values of resistance. This comparison is shown in Table 4. Even when better values of resistance are known there were still differences between the calculated phase-change times and the measured phase-change times. This variation could come from the assumption that the sample was a uniform block of phase-change material, when in fact the sample was a composite of foam and phase-change material. This composite has void spaces that reduce the heat transfer to the phase-change material from the foam. It is also possible that the phase-change material shrunk in the process of solidifying, leaving a poor contact between the foam and the phase-change material, which would inhibit the heat flow into the phase-change material, causing the phase change to take longer than the simple case calculated. Another possible reason for the difference in the predicted phase-change time and the actual phase-change time is that the plateau was not at constant temperature. The sample was increasing in temperature during the phase change. This increase in temperature pulls heat energy away from the phase change causing the phase change to take longer than predicted by changing the energy balance from Eq. (12) to

$$q_{\text{in}}t - (q_{\text{out}}t + q_{\text{loss}}t) = M_{\text{PCM}}h_{\text{sf}} + (M_f c_f + M_{\text{PCM}}c_{\text{PCM}})\frac{\mathrm{d}T}{\mathrm{d}t} \tag{17}$$

Even though the time constants and the phase-change times show the accuracy of the prediction, it does not always clarify the complete solution. To show the complete solution the transient temperature profile prediction was compared with the experimental results for each case. A representative version of this comparison is shown in Fig. 9 for the experimental case of Poco foam infiltrated with acetamide, placed in contact with the cold plate, and with a boundary temperature of $T_H = 135$°C. The measurements from three thermocouples have been plotted against the theoretical prediction. The fifth curve, Experimental R, is the temperature curve calculated using the theoretical method, but replacing the resistance networks (Figs. 4 and 5) with experimentally determined resistances. The Experimental R curve is closer to the experimental foam temperature curve reinforcing the importance of knowing the resistance accurately.

The final parameter predicted in the Test Configuration and Theory section was the power into the foam. This predicted power into the foam is plotted in Fig. 10 with the power into the foam determined from the experiment for the same case as that in Fig. 9. A third curve, Experimental R, is plotted using the experimentally determined resistances rather than the theoretical resistance calculated from the resistance network. This plot shows the analytic method can approximate the actual power into the foam if the resistance is known accurately.

More data can be found in [7].

IV. Conclusion

The transient response of the foam and phase-change material was investigated by application of a step temperature heat load. The experimental response was an approximate first-order exponential curve with a plateau during the phase change. A simple analytic prediction of this response was developed, and whereas not exact, it does provide a rough estimate of the response. This prediction would be useful for engineers considering the use of this type of system. The experimentally determined resistance was also used in the theoretical prediction to show that more accuracy can be gained in the prediction if better values of the resistance are known.

This study also considered the bonding of a carbon–carbon plate to carbon foam. It was found that a 0.025 cm thick bond could be obtained consistently with a graphitic bonding material through the use of basic techniques and a heated cure cycle. As also noted from other research results, poor conductivity of bonding material and contact resistances offer the largest uncertainty between theory and experiment and naturally tend to inhibit heat transfer the most.

The highest infiltrations rates were achieved by placing the foam in a pool of liquefied phase-change material, pulling a vacuum on the foam and phase-change material, and releasing the vacuum once the foam had finished releasing air but while the phase-change material was still liquefied. This allowed the atmospheric pressure to force the phase-change material into the pores of the foam.

References

[1] Klett, J. W., and Burchell, T. D., "Pitch-Based Carbon Foam Heat Sink with Phase Change Material," United States Patent No. 6,780,505, Aug. 2004.

[2] Hagar, J. W., and Lake, M. L., "Novel Hybrid Composites Based on Carbon Foams," *Materials Research Society Symposium Proceedings*, Vol. 270, Materials Research Society, 1992, pp. 29–34.

[3] Lee, C. W., and Lafdi, K., "Stabilization Study of Carbon Foam," *35th SAMPE Technical Conference*, Dayton, OH, 2003.

[4] Hale, D. V., Hoover, M. J., and O'Neil, M. J., "Phase Change Materials Handbook," NASA CR-61363, Sept. 1971.

[5] Incropera, F. P., and DeWitt, D. P., *Fundamentals of Heat and Mass Transfer*, 4th ed., John Wiley & Sons, New York, 1996.

[6] Cao, Y., and Ponnappan, R., "A Liquid Cooler Module with Carbon Foam for Electronics Cooling Applications," AIAA Paper 2004-492, Jan. 2004.

[7] Wierschke, K., "Thermal Characteristics of Pitch-Based Carbon Foam and Phase Change Material," MS Thesis No. AFIT/GSS/ENY/05-M05, Air Force Institute of Technology, Wright–Patterson AFB, OH, 2005.